

A COMPUTER VISION APPROACH TO ESTIMATE THE LOCALIZED SEA STATE

Aleksandar Vorkapic, Miran Pobar, Marina Ivasic-Kos

Faculty of Informatics and Digital Technologie, & Centre for Artificial Intelligence, University of Rijeka, 51000 Rijeka, Croatia

a.vorkapic@icloud.com; mpobar@uniri.hr; marinai@uniri.hr

Abstract

This research presents a novel application of computer vision (CV) and deep learning methods for real-time sea state recognition aiming to contribute to improving the operational safety and energy efficiency of seagoing vessels, key factors in meeting the International Maritime Organization's carbon reduction targets. In particular, our work focuses on utilizing sea images in operational envelope captured by a single stationary camera mounted on the ship bridge, which are used to train deep learning algorithms for automatic sea state estimation based on the Beaufort scale. To recognize the sea state, we used 4 state-of-the-art neural networks with different characteristics that proved useful in various computer vision tasks: Resnet-101, NASNet, MobileNet_v2 and Transformer Vit -b32. Furthermore, we have defined a unique large-scale dataset, collected over a broad range of sea conditions from an ocean-going vessel prepared for machine learning. We used transfer learning approach to fine-tune the models on our dataset. The obtained results suggest promising potential for this approach to complement traditional methods, particularly where in-situ measurements are unfeasible or interpolated weather buoy data is insufficiently accurate.

This study sets the groundwork for further development of machine learning-based sea state classification models to address recognized gaps in maritime research and enable safer and more efficient maritime operations.

Key words: energy efficient shipping, computer vision, waves estimation, neural networks, real-time monitoring

1. Introduction

Accurate assessment and anticipation of sea states are important for ensuring navigational safety and minimizing a ship's energy consumption. Predicting sea conditions allows for the planning of safer and more fuel-efficient routes, thereby avoiding regions with potentially hazardous weather that could increase Greenhouse Gas (GHG) emissions from excessive carbon-based fuel consumption. The International Maritime Organization (IMO) leads such initiatives in maritime sector, targeting a reduction of GHG emissions and fostering global climate change mitigation. Specifically, the IMO's GHG emissions strategy sets a target to decrease the carbon intensity of all ships by 40% by 2030, using 2008 as a benchmark. The short-term measures promoted to reach these targets include adopting more energy-efficient vessels to reduce GHG outputs. Fuel consumption for propulsion constitutes the largest portion of a vessel's total energy distribution; therefore, optimizing propulsion leads to the most significant energy savings (Bouman et. Al 2017; Lindstad et al. 2015a, Taalat et al 2022.). Effective navigation routes mapped out with consideration for adverse weather, can further mitigate the impact on a ship's performance (Wu, et al 2021). By integrating weather and oceanographic data into their strategic planning, ship operators can enhance navigational safety, optimize operational costs, and lessen the environmental footprint, advancing towards the IMO's set energy efficiency and sustainability in maritime operations (Ruth & Thompson, 2022).

Autonomous maritime operations are gaining interest in maritime-related research, offering potential to lessen human error and enhance both safety and efficiency. Computer vision (CV) is emerging as key technology for autonomous shipping, enabling ships to detect and respond to their environment in real-time (Mosbauer et al., 2019; Quiao et al., 2021). By employing CV-based sea state recognition, ships can make informed decisions and adjust their operations, leading to safer and more efficient operations. Additionally, CV also brings promise to the fields of weather and oceanographic forecasting. The ability to recognize sea states in real-time can contribute to more accurate, timely forecast, enabling marine industry to plan navigation more effectively and safely.

There has been interest in the application of machine learning techniques to determine sea states, aiming to achieve more accurate and reliable results. Nielsen et al. (2015) presented new concept for shipboard sea state estimation through measurement of wave height, wave period, and wind speed. The study provides insights into the use of sensor data for sea state estimation and highlights the significance of accurate sea state identification for maritime safety. Tu et al. (2018) developed a sea state classification method based on ship movement four-degree-of-freedom (DoF) ship motion data (surge, sway, roll, and yaw). The data were pre-processed, decomposed into 20 categories per DoF, and 11 statistical features were extracted to train their model. Their classification system was built in three layers: the first used adaptive neuro-fuzzy interference system classifiers for each category, the second involved random forest classifiers, and the third applied a bias-compensating method for averaging the outputs with reported accuracy ranged from 74.4% to 96.5%. Notably, this method is dependent on ship motion sensor data and did not extend to the sea state classification through visual sea images. Ampilova et al. (2019) applied multifractal methods for the analysis of sea surface images for sea state determination. The study provides insights into the use of fractal-based approaches for sea state identification and highlights the importance of considering the multiscale nature of sea surface patterns. Cheng et al. (2019) developed a novel time-frequency image-based approach for sea state estimation using motion data from dynamically positioned vessels. The study utilized simulated ship movement data from nine sensors to train and test a convolutional neural network (CNN) and highlighted the potential of data-driven approaches for sea state estimation. By employing short-time Fourier transform, each sequence of data from the sensors was converted into a single spectrogram. The sea states were bifurcated into 5 categories, and the proposed 2D CNN model was trained to classify them using the spectrogram. The results were compared to long-short term memory architecture (LSTM) and 1D CNN models, with the proposed model achieving the highest classification accuracy of 94%. However, the study did not report the number of spectrogram instances per class and in the overall dataset, as well as the per-class classification accuracy. Consequently, the model's generalization ability across various classes remains unknown. Liu et al. (2021) proposed a sea state classification method using a LeNet-based model and sea clutter radar data from two sources. The datasets covered three sea states with significant wave heights ranging from 0.5 m to 4 m. Separate models were trained and tested on the datasets, resulting in classification accuracies of 95.75% for states 3–4 and 93.96% for states 4–5. The lower accuracy (93.96%) was attributed to limited buoy measurement calibration points for the corresponding sea clutter radar data. Although the study claims strong generalization ability, the models were tested in a small temporal and geographical setting, and high-class imbalance was observed in the datasets. Consequently, the models may exhibit bias towards the majority class. Zhang et al. (2021) utilized a residual network, ResNet-152 model to classify sea states from optical images of the sea surface. The study divided sea states into 10 categories based on ship movement and wave forms, using video data collected from a ship-mounted visual-range video camera. An unusual data split ratio of 82:18 was employed for training and validating the model, which achieved a validation accuracy of 89.3%. However, the study does not report any measure to quantify the testing accuracy of the proposed method, nor does it mention sea-state-wise and overall classification accuracy. Additionally, the method's division of sea states into 10 categories does not follow recognized standards such as the Beaufort or Douglas scales. Consequently, the study has limited significance. Recent study by Umair et al. (2022) introduced a deep learning model for sea state classification using visual-range sea images in four sea states ranging from 1 to 4 on the Beaufort scale. The model

demonstrated high accuracy rate of 97.8% on a test dataset, showing promising results. The study highlights the potential of deep learning in sea state recognition and the relevance of visual-range imaginary in such applications. Another recent study was conducted by [Mittendorf et al. \(2022\)](#), who used in-service data from a container vessel to compare the performance of various machine learning algorithms for sea state identification. They found that a random forest algorithm achieved the best results, with an accuracy of 90.5% on a test dataset. The study provides valuable insights into the use of machine learning for sea state identification based on in-service data. [Rus et al. \(2022\)](#) developed the HIDRA2 model for sea level and storm tide forecasting in the northern Adriatic, using a deep-learning ensemble trained on a large dataset of sea level and meteorological data. HIDRA2 outperformed other state-of-the-art models, achieving a root mean square error of 0.089 m for sea level and 0.111 m for storm tides. Including seiche information significantly improved the model's performance. HIDRA2 represents an important advance in sea level and storm tide forecasting, with implications for coastal management and disaster preparedness in the region.

The relevant research has revealed challenges in accurately identifying sea states, particularly in the diverse and dynamic conditions encountered in real-environment applications. A notable gap is the lack of comprehensive datasets that reflect the navigating range of sea states. These present opportunities for further research to harness CV techniques and develop algorithms that can effectively interpret sea imagery within the operational envelope.

The specific objective of this research is to address the aforementioned gaps by creating and developing a CV algorithm capable of accurately detecting and categorizing various sea states in real operational conditions. This approach employs cameras and deep learning algorithms to automatically classify waves, providing a standardized measure of sea state. It can be particularly valuable in areas where traditional methods, such as in-situ measurements, are not feasible or cost-effective, or where interpolated values from weather buoys are insufficiently accurate ([Vorkapic et al., 2021-a/b](#)). The CV-based sea state classification approach could potentially be used alongside physical methods to provide a more comprehensive understanding of seagoing dynamics.

The main contributions of our work can be summarized as follows:

1. Original custom dataset with 8 sea state classes according to Bf 1 to 8 prepared for supervised machine learning
2. Fine-tuned ResNet, MobileNet, ViT and NASNet deep models for sea state recognition on our original data set
3. Proposal of image sampling strategies in the case of texture recognition or small object detection and analysis of the results according to the sampling strategy
4. Comparison of model performance according to standard metrics and selection of the most suitable models for the task of recognizing the state of the sea.

The paper is structured as follows: Section 1. presents the problem, research objectives and provides review of the previous research; Section 2. presents the background of dataset, tools, evaluation methods and modelling process; Section 3. validates machine learning methods and illustrates the results obtained, followed by Section 4., which concludes the paper.

2. Material and methods

The Beaufort scale is a traditional method for estimating sea state, linking wind speed to observed conditions at sea or on land. It categorizes the sea states into 13 classes (0-12) based on the corresponding wind speeds and provides a brief description of the visual features of each state. The process is typically carried out through visual observation from the bridge, but the potential for human error makes computerized sea state classification models an appealing

alternative. Utilizing CV for sea state recognition based on the Beaufort scale offers an efficient method for monitoring sea state and wave conditions.

2.1. Dataset collection

In order to train the models for sea state recognition, as part of this research study, an extensive set of data that includes the target sea states had to be first collected and then annotated and prepared for machine learning. The collected raw data encompasses 119 video recordings, which collectively constitute 39.61 gigabytes of high-definition visual data. These recordings were made in 11 distinct geographic locations, ensuring a broad coverage of maritime environments. Utilizing a stationary camera with a resolution of 3840x2160, the footage was captured without human intervention and saved using the HEVC codec. The positioning of the camera on the left bridge wing of the vessel afforded a panoramic view of the sea and included segments of the ship, the wake, and the distant horizon. The height at which the recordings were captured varied with the vessel's loading condition: the bridge wing stood at 38.12 meters above sea level while in cargo, and 40.32 meters when in ballast.

Given the inherent challenges in documenting sea states above 6-7, the vessel of choice for this study was a large ocean-going ship, specifically selected for its operational capabilities in the harsh winter conditions and tumultuous seas. This selection was aimed at maximizing the probability of capturing recordings of the higher sea states. The video recordings were conducted on an 89,432 DWT and 173,998 m³ liquefied natural gas transport vessel, akin to the vessels from a 174km³ series previously constructed by Korean shipbuilders. The recording period spanned from 12/02/2022 to 24/12/2022, during which the vessel was both in navigation and at anchor, to ensure a diverse representation of sea states could be captured and analyzed.

The exact geographic locations of the recordings are shown in Figure 1.

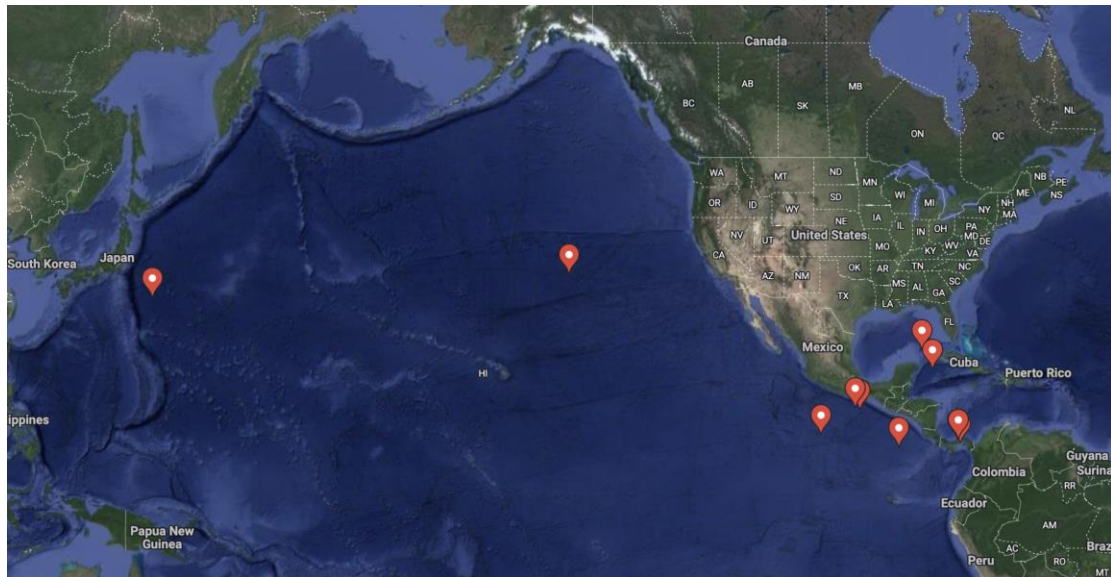


Figure 1. Map of sea state image acquisition locations.

Figure 2 illustrates two representative frames of the video footage from which crops were extracted for subsequent analysis. These frames were selected to demonstrate the type of raw visual data obtained from the stationary camera mounted on the vessel during navigation or when anchored. The image showcases the specific section of the maritime environment that was consistently captured across the various recordings. In subsequent processing, individual crops were extracted from such frames to ensure that the further analysis would be based on

consistent and relevant segments of the visual data, focusing on key features of the sea state, and excluding e.g. most of the sky or ship's wake.



Figure 2. Sample frames for maritime video dataset for sea state analysis.

For each recorded video, the sea state in Beaufort scale was estimated by human experts, as would be during regular ship operations. The estimated sea state values according to the Beaufort scale were compared with the measured wind speed using the ship's anemometer, and they mostly matched. The basic data about the collected videos for each sea state is shown in Table 1.

Table 1. Statistics of collected videos for sea states from 1-8 Bft.

Sea state	1	2	3	4	5	6	7	8
No. sessions	6	7	7	7	7	4	3	3
No. frames	19.173	24.101	14.030	33.063	46.303	16.282	15.094	6.393
Total duration (m:s)	5:20	6:42	3:54	9:11	12:52	4:31	4:12	1:47

We use the Beaufort scale, which traditionally ranges from 0 to 12, indicating a total of 13 distinct sea states, as the guiding framework for classification in this work. However, within the scope of our dataset, we were successful in capturing sea states spanning from 1 to 8. The absence of state 0 and those beyond 8 in our dataset is attributable to operational challenges in obtaining such data; state 0, or 'calm' conditions, are relatively rare in the operating environment of the vessel, and states above 8 are exceedingly difficult to capture due to their severity and the associated safety concerns. Consequently, our dataset comprises eight classes, corresponding to sea states 1 through 8 on the Beaufort scale which provides a significant range of conditions for analysis given that, as a rule, ships navigate in these conditions. Sea state 8 is already considered borderline for operational safety and energy efficiency on the subject vessel, and sea states above 8 are actively avoided.

2.2. Dataset preparation

The basic prerequisite for the implementation of this research is the definition of a customized dataset intended for the development and validation of machine learning models aimed at sea state analysis that is formed from the collection of video recordings. From the collected raw video material, a customized data set for training and testing the model was constructed.

The initial collection of videos was found to be imbalanced with respect to the total number of frames, with certain classes containing more data than others. To form the balanced dataset from the initial uneven quantity of data for each sea state, and to distill the video data into a form more

suitable for analysis, a systematic sampling approach was employed. This process involved the selection of frames at regular intervals from the recorded footage, so that the number of frames for each sea state is about 750. From each chosen frame, a segment with dimensions of 331x331 pixels was extracted from the bottom-left corner of the frame (Fig. 3). These segments were then incorporated into the training or test subsets, depending on whether they were extracted from videos in the training or testing subsets. This dataset was named UNIRI-SeaState-LL. An illustrative set of samples representing each sea state in the resulting dataset is shown in Figure 5.



Figure 3. The size and location of cropped portion of initial frame included in the dataset UNIRI-SeaState-LL (Yellow frame marked A). Green frames marked B represent some possible locations of crops included in the dataset UNIRI-SeaState-R.

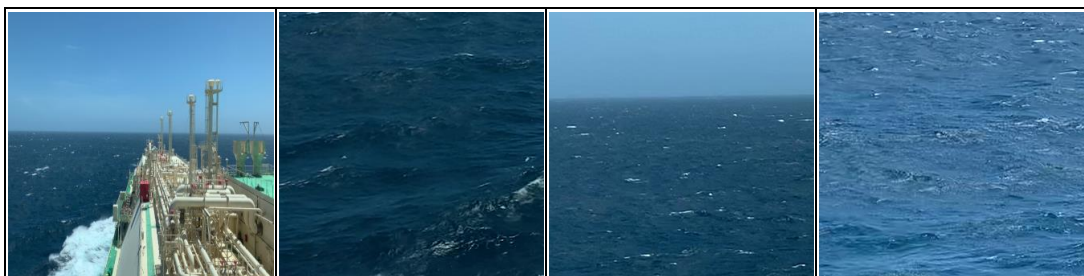


Figure 4. Example of sea state 7 in a) resized image b) crop from the bottom-left part of the image, c) crop near the horizon line, d) crop from a random part of visible sea.

The rationale behind the frame size and sampling frequency is directly correlated with the model input size and the height from which the sea was recorded. Resizing images to fit the input dimensions of our models resulted in the loss of details needed for accurate sea state determination (Fig. 4a). Furthermore, the recordings were obtained from heights of 38.12 meters and 40.32 meters, depending on the vessel's loading condition. At such elevations, the discernible differences between adjacent sea states are marginal and can be challenging to detect. To overcome this, we explored various image sampling strategies that would allow us to preserve important features within the constraints of model input sizes, namely cropping from the bottom-left corner (Fig. 4b), cropping near the horizon (Fig. 4c) and random crops within the part of the image with the sea visible (Fig. 4d). This zoomed perspective is instrumental in

enhancing the visibility of features that are critical to the accurate classification of sea states, thereby facilitating a more nuanced analysis conducive to the objectives of this study. The crops near the horizon line contained less visible detail and were difficult to obtain reliably with significant proportion of sea to the sky, so were not included in the further experiments.

In the development of the dataset, we have also explored a variant where the sample is taken from a random position to the left of the ship's hull (Fig. 3). This variant of the dataset is named UNIRI-SeaState-R.



Figure 5. Examples of extracted sea state images. Top row: states from 1 to 4 Bft. Bottom row: states from 5 to 8 Bft.

Table 2. Class Distribution Balance Across Different Cropped Image Datasets

Dataset	Classes								Total images
	1	2	3	4	5	6	7	8	
UNIRI-SeaState-R	750	750	737	750	750	744	710	766	5.957
UNIRI-SeaState-LL	750	736	750	750	750	758	706	770	5.970

Table 2 details the resultant class distribution for both datasets. It provides a numerical overview of how images were equitably distributed across the classes to facilitate a balanced representation in line with the Beaufort scale's defined sea states.

2.3. Model architectures

In the development of models for sea state classification, our selection of model architectures was guided by the proven efficacy of contemporary classifiers in the realm of machine learning. We chose to integrate renowned architectures such as ResNet-101 (He et al. 2016), NASNet (Zoph et al. 2018), MobileNet V2 (Sandler et al. 2018), and Vision Transformer (Kolesnikov et al. 2021), all of which have been trained on extensive datasets like COCO (Lin et al. 2014) or ImageNet (Deng et al., 2009). These models have not only excelled in benchmark tests but have also set the standard for accuracy in diverse applications.

We adopted the architecture of these classifiers, and used fine-tuning on our dataset from the pre-trained weights to build models that can reliably interpret the complex and dynamic nature of maritime environments.

The used model architectures are described in brief in the following subsections.

ResNet-101

ResNet-101 is a deep convolutional neural network (CNN) architecture designed to address the vanishing gradient problem in very deep networks. It belongs to the ResNet (Residual Network) family, which was introduced by Microsoft Research in 2015. The "101" in its name refers to the number of layers in the network. The main innovation in ResNet is the introduction of residual blocks, which include skip connections or shortcuts to facilitate the flow of gradients during training. This helps mitigate the vanishing gradient problem and allows for the training of significantly deeper networks.

ResNet-101 has proven to be highly effective for various computer vision tasks, including image classification, object detection, and segmentation. Its architecture has become a foundation for the development of even deeper and more complex neural networks, contributing to advancements in the field of deep learning.

The basic building block of ResNet-101 is called the bottleneck residual block (Fig. 5). The block comprises three layers, a 1×1 convolution, 3×3 convolution, and another 1×1 convolution layer, where the first 1×1 layer reduces, and the final 1×1 layer restores the dimensions, leaving the middle 3×3 layer with smaller input/output dimensions, effectively reducing the computational cost.

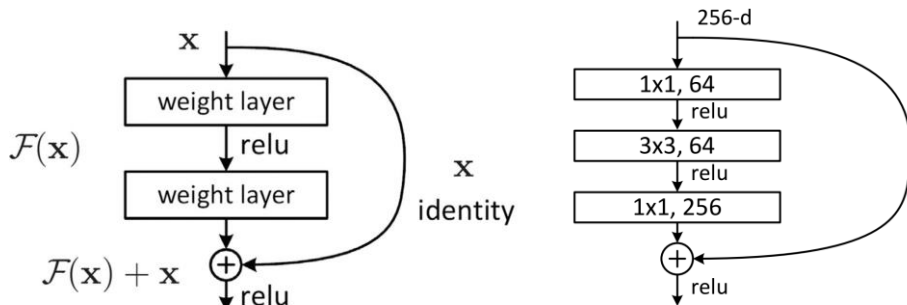


Figure 6. A "bottleneck" building block for ResNet-50/101/152 (He et al. 2016)

The key element of the residual block is the shortcut connection, or residual connection, which adds the input of the block directly to the output. This shortcut allows the gradient to flow directly through the network.

ResNet-101 has a total of 33 such building blocks, and with additional 2 layers at the input, contains a total of 101 layers.

At the end of the network, ResNet-101 employs a global average pooling layer followed by a fully connected layer with a softmax activation function for classification tasks.

NASNet

Similar to ResNet, NASNet architecture is formed by stacking a fixed structure of layers that form basic building blocks to form the complete network. However, the structure of the building blocks is not designed manually but discovered automatically using a reinforcement learning-based process, called neural architecture search (NAS). The neural architecture search process

employs a reinforcement learning agent, guiding the selection of operations within the building blocks (cells) based on their performance in specific tasks.

The building blocks of NASNet-A were determined on the classification task using the CIFAR-10 dataset and employed successfully for classification on other datasets like ImageNet.

The architecture includes two types of cells: reduction cells and normal cells (Fig. 6.). Reduction cells downsample spatial dimensions, reducing the spatial resolution, and normal cells maintain the spatial resolution.

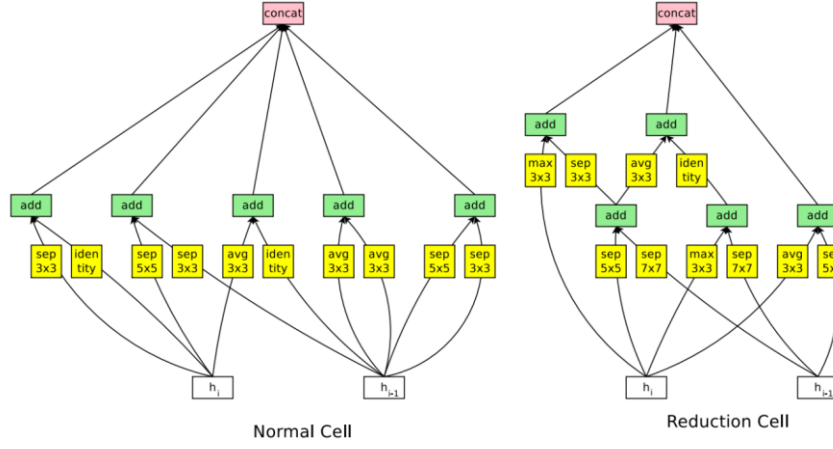


Figure 7. Normal and Reduction cells of NASNet. (Zoph et al. 2018)

NASNet-A focuses on efficiency and is designed to achieve state-of-the-art performance with fewer parameters and computations compared to manually designed networks.

The neural architecture search process considers multiple objectives simultaneously, such as accuracy, model size, and computational efficiency. This multi-objective optimization results in a balanced trade-off between performance and resource requirements.

NASNet-A has demonstrated competitive performance on benchmark datasets, achieving top-tier accuracy in image classification tasks while being computationally efficient.

Based on the NASNet-A normal and reduction cells, many configurations of the network with different numbers of stacked cells and different number of filters in the initial convolutional cell have been used, offering trade-offs between computational complexity and performance.

In this work, a configuration with four repetitions of normal cells between reduction cells and 1056 filters in the initial layers was used. This is a lightweight configuration with only about 5 million parameters, suited for mobile and edge computing devices.

The architecture aims to strike a balance between achieving satisfactory performance and minimizing the computational resources needed for inference on mobile platforms.

MobileNet V2

MobileNetV2 is a lightweight convolutional neural network architecture designed for environments with constrained resources such as mobile and edge devices. It is an evolution of the original MobileNetV1, focusing on design simplicity and improved performance.

MobileNetV2 introduces the new inverted residual layer block that uses a lightweight depthwise separable convolution followed by linear bottlenecks (Fig. 7). The depthwise separable convolution is computationally much simpler than the full convolution while retaining good

performance. The bottleneck layer is a 1×1 convolution with linear activation function that helps preserve information flow. Similar to the building block of ResNet, the inverted residual layer of MobileNetV2 features skip connections, however here the skip connections are between the input and the lower-dimensional bottlenecks. In each inverted residual block of MobileNetV2, an expansion layer within the depthwise separable convolution allows for an increase in the number of channels, controlled by the expansion factor t , enabling the network to capture more complex features. The linear bottleneck layer following the depthwise separable convolution reduces the dimensionality back to facilitate information flow through skip connections.

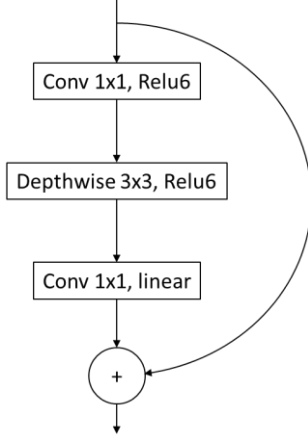


Figure 8. Inverted residual block of MobileNetV2, adopted from (Sandler et al. 2018)

Collectively, these features contribute to its suitability for deployment on mobile and edge devices, enabling inference with reduced computational demands.

Vision Transformer

The Vision Transformer (ViT) model is a departure from the conventional convolutional neural network-based models. ViT leverages the transformer architecture, originally designed for natural language processing (NLP), and applies it directly to image data. As the standard Transformer receives a 1D sequence of token embeddings, the 2D images are first reshaped to conform to the expected shape. The input images are divided into fixed-size non-overlapping patches and flattened to 1D. Subsequently the sequences of flattened pixel values are treated as “tokens” in NLP applications. The patches are linearly embedded into high-dimensional vectors, forming the input sequence for the transformer.

ViT uses a standard transformer architecture, consisting of self-attention mechanisms and feedforward neural networks. The self-attention mechanism enables the model to capture global dependencies within the input sequence. Since transformers do not inherently understand the spatial layout of the input image, the positional information in form of positional embeddings are explicitly added to the patch embeddings to preserve the spatial information of the image.

Furthermore, the lack of translation equivariance and locality, that is a feature of CNNs, hinders the capability of the transformer to generalize well when trained on insufficient amounts of data.

Smaller datasets can be used successfully using fine-tuning from models that are pre-trained on larger datasets.

The ViT architecture is scalable, and in this work, a the ViT-b32 variant is used. This is a smaller model with about 87 million parameters, in comparison with ViT-Large variant with more than 300 million parameters. The number of parameters is still much larger than other networks tested, especially the NasNet Mobile and MobileNetV2 architectures.

2.4. Experiment setup

The four model architectures described above were each trained on the two variants of the dataset, UNIRI-SeaState-lower-left-331 and UNIRI-SeaState-random-331, resulting in eight total trained models. All models were trained in two steps from initial weights pretrained on the Imagenet dataset. On top of the base models, a global average pooling layer and a dense layer with linear activation was used, except for the ViT-b32 model, where a dense layer with GELU activation function was used before the final prediction layer with linear activation.

First, the models were trained using transfer learning for 30 epochs, with weights in all layers of the network frozen except for the final (output) dense layer and using the Adam optimizer. Then, in the second step, a number of layers was unfrozen to allow fine-tuning of a part of the base network on new data. The number of trainable parameters in this step is shown in Table 3 for each architecture. For the second step, RMSProp optimizer was used with the number of training epoch varying from 200 to 1000 between different architectures, chosen according to the point where there was no further improvement in the training accuracy. In the first step, learning rate of 0.0001 was used. In the second step, progressive learning rate was used, with base learning rate of 0.0001 and with reduction on plateau by a factor of 5 down to minimum learning rate of 1e-6, with patience of 30 epochs and a threshold of validation accuracy improvement of 1e-6.

Batch size for all models was 250, except for Vit, where 200 images were used in a batch due to memory constraints. As an example, training and validation accuracy for ResNet trained on UNIRI-SeaState-random-331 dataset is shown in Figure 8.

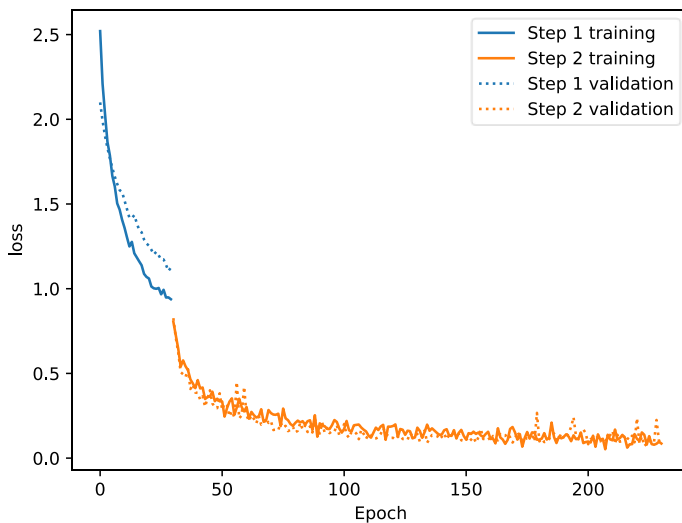


Figure 9. Training and validation loss for Resnet-101 trained on UNIRI-SeaState-random-331.

A summary of model sizes and parameters is shown in Table 3.

Table 3. Summary of Model Architectures.

Deep Network Architecture	Neural	Total parameters	Trainable parameters	Training epochs
ResNet-101		42,7 M	24,8 M	230
Vit -b32		87,5 M	21,3 M	230
MobileNetv2_1.00_224		2,7 M	0,7 M	430

NasnetMobile	4,3 M	1,6 M	1030
--------------	-------	-------	------

The input image size for all models was 224x224 pixels, while the images in the dataset were sized 331x331 pixels. This discrepancy was handled by further cropping the input image both during training and during testing, however, during testing the crop position was always the same, from the center of the image, to ensure repeatability, while during training the crop position was random and was in effect a form of data augmentation.

During training, the following data augmentations were used:

- *Random cropping*: As noted above, random 224x224 crops were chosen from the initial 331x331 image in the dataset (Fig. 9). Note that depending on the dataset, the 331x331 images are themselves either random crops from the initial whole video frame, or crop from the fixed bottom-left position. This augmentation was always applied.

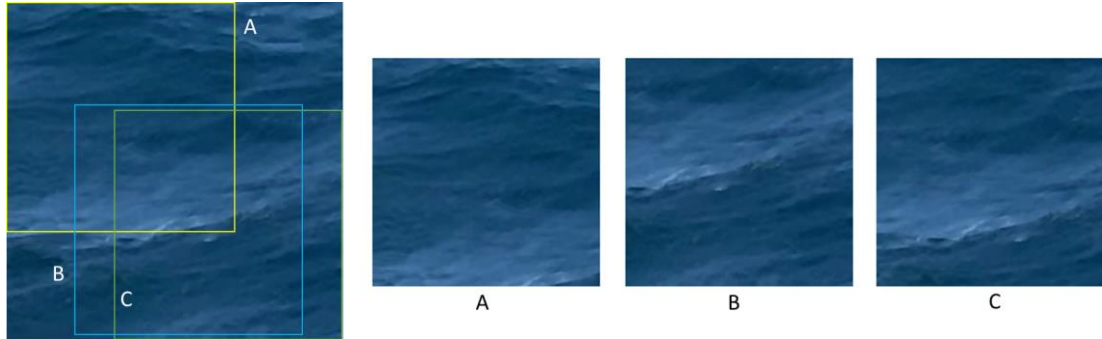


Figure 10. Example of cropping data augmentation. A, B and C show three random crop regions and corresponding cropped images.

- *Motion blur*: A horizontal motion blur was applied to the batch with 50% probability by convolving the image with a horizontal 7x7 motion blur kernel. This was chosen as similar blur was often observed in the original images due to camera panning motion.
- *Horizontal flip*: images were flipped horizontally with 50% probability.
- *Random brightness and contrast adjustments*: Brightness was randomly scaled with a factor in the range [-0.2..2] and contrast was adjusted with a random factor in the range of [0.5..1.5]
- *Random rotation*: images were randomly rotated in range of angles from -0.2pi to 0.2pi radians.
- *Random grayscale conversion*: Images were converted to grayscale with 20% probability.

In total 8 models were trained, one of each architecture for both datasets.

In order to test the generalization performance, the best performing model was tested on the MU-SSiD (Umair et al. 2022) dataset, which contains images of sea states limited to the range of 1-4 Bft. Additionally, the ResNet model that performed best on our dataset was trained on the MU-SSiD dataset, with identical settings and evaluated on both datasets.

2.5. Evaluation Metrics

In the evaluation of our machine learning models, we have adhered to the standard metrics that are widely recognized in the field for assessing performance. These metrics are precision, recall, and the F1 score, each calculated for every individual class to capture the models' effectiveness at correctly identifying the distinct sea states.

Precision, also known as the Positive Predictive Value (PPV), is the proportion of true positive cases among all cases predicted as positive. It is a measure of a model's accuracy in identifying cases as belonging to a particular class. A higher precision indicates a lower rate of false positives. The formula for precision is given as:

$$Precision = \frac{TP}{TP + FP}, \quad (1)$$

where TP represents the number of true positives, and FP denotes the number of false positives.

Recall (also known as sensitivity or True Positive Rate, TPR) assesses the model's ability to correctly identify all actual instances of a given class. It is particularly critical in scenarios where failing to detect a condition could have serious implications, and it addresses the question: Of all the actual sea states of a class, how many were identified?

$$Recall = \frac{TP}{TP + FN}, \quad (2)$$

where FN is the number of false negatives. Both precision and recall are balanced by the F1 score, which is the harmonic mean of the two and is used when one needs to consider both false positives and false negatives equally.

The F1 serves as a balanced metric that harmonizes the precision and recall of a classification model into a single figure. This score is of paramount importance when one needs to consider the trade-off between the precision (or Positive Predictive Value, PPV) and the recall (True Positive Rate, TPR), such as in cases where both false positives and false negatives carry similar consequences. Moreover, the F1 Score is particularly informative in the presence of imbalanced class distributions, where the cost of misclassification can differ across classes. The F1 Score is calculated using the formula:

$$F1 = \frac{2 \times PPV \times TPR}{PPV + TPR}. \quad (3)$$

In this formula, PPV is the number of true positive results divided by the number of all positive results predicted by the classifier, and TPR is the number of true positive results divided by the number of all actual positives. The F1 score effectively captures both the precision and robustness of the classifier's positive predictions.

For an overarching assessment of the model performance across all classes, we utilize Accuracy, which gives us the ratio of correctly predicted observations to the total observations. This is complemented by the Macro Average, which calculates metrics for each class independently and then takes the average, treating all classes equally.

$$\text{Macro Average} = \frac{1}{n} \sum_{\text{class}=1}^n \text{metric rate for each class}, \quad (4)$$

This means it does not take label imbalance into account. Conversely, the Weighted Average takes the label imbalance into account and calculates metrics for each class proportionally to its presence in the dataset.

$$\text{WA} = \frac{\sum_{\text{class}=1}^n \text{metric rate} * \text{numer of instances per class}}{\text{total number of instances}}, \quad (5)$$

By employing both macro and weighted averages, we ensure a comprehensive understanding of the model performance across classes with varying representation in the dataset. This dual approach allows us to recognize excellence in models' classification capabilities while also identifying potential areas of bias or weakness, particularly in classes that are underrepresented or more challenging to predict.

3. Results and Discussion

In our research, we conducted two distinct experiments to assess the efficacy of our selected machine learning models in classifying sea states. The first experiment employed images sampled from random positions within the video footage, creating a dataset reflective of diverse perspectives. This dataset, referred to as "UNIRI-SeaState-R", is comprehensive, encompassing a total of 5,957 images, as previously detailed in Table 1. The second experiment, on the other hand, utilized images extracted from a fixed position in the video, specifically from the lower-left area relative to the ship's hull. This dataset, termed "UNIRI-SeaState-LL", consists of 5,970 images, ensuring consistency in the visual information presented to the models.

Both datasets were split into training and testing sets, with the training set comprising a significant majority (shown in Table 2). The testing set was curated to evaluate the models' performance objectively, as it contained previously unseen images that were representative of real-world conditions. When selecting images for testing, care was taken to ensure that the images were taken from videos that were not used for training and that the set was balanced.

Table 4. Performance Metrics for Models Trained and Tested on Images from Random Positions (UNIRI-SeaState-R Dataset)

Fine-tuned models	Metrics	Classes								Accuracy	Macro avg	Weighted avg
		1	2	3	4	5	6	7	8			
ResNet	precision	1.000	0.904	0.538	0.923	1.000	0.802	0.963	0.878		0.876	0.911
	recall	0.930	0.979	0.935	0.864	0.801	0.819	1.000	0.905	0.881	0.904	0.881
	f1-score	0.964	0.940	0.683	0.893	0.889	0.810	0.981	0.891		0.881	0.888
ViT	precision	0.989	0.866	0.558	0.967	0.950	0.698	0.975	0.886		0.861	0.895
	recall	0.935	0.983	0.886	0.707	0.866	0.867	0.996	0.979	0.868	0.902	0.868
	f1-score	0.961	0.921	0.685	0.817	0.906	0.773	0.985	0.930		0.872	0.872
MobileNet	precision	0.970	0.417	0.337	0.544	0.589	0.275	0.727	0.341		0.525	0.566
	recall	0.516	0.858	0.337	0.305	0.428	0.460	0.899	0.821	0.502	0.578	0.502
	f1-score	0.674	0.561	0.337	0.391	0.496	0.344	0.804	0.481		0.511	0.501

NasNet	precision	0.960	0.910	0.494	0.887	0.843	0.472	0.991	0.789		0.793	0.823
	recall	0.976	0.907	0.776	0.563	0.733	0.794	0.983	0.947	0.781	0.835	0.781
	f1-score	0.968	0.908	0.603	0.689	0.784	0.592	0.987	0.861		0.799	0.787

Upon reviewing the performance metrics presented in Table 4, it is evident that ResNet achieves the highest overall accuracy, closely followed by Vision Transformer (ViT). This high accuracy demonstrates the models' ability to correctly classify sea states across the dataset. Notably, the performance of NASNet and MobileNet is marginally lower, which could be attributed to their significantly smaller number of parameters—approximately ten times less than ResNet—manifesting in a roughly 10% drop in accuracy for NASNet.

All models exhibit the highest F1 scores for class 7, despite it not being the most represented class in the dataset. This suggests that the images for class 7 are of sufficient quality to facilitate effective learning by the models. Conversely, all models perform the least effectively on class 3, followed by class 6, indicating these classes may benefit from a more diversified or expanded set of training examples to enhance model learning.

The class-wise variation in precision and recall further illustrates the performance of each model. Class 7, with its high precision across all models, suggests that the class contains distinctive, well-captured features conducive to accurate classification. High recall scores in other classes indicate successful identification of most positive examples within those classes.

In sum, ResNet's superior accuracy, alongside its strong macro and weighted average scores, showcases its robustness and adaptability across varied sea states. In comparison, the smaller architectures of both NasNet and MobileNet still deliver respectable average precision and recall, but with significantly lower scores for some classes.

On the set of images sampled from a fixed position, all models show better results than in the case of random sampling (Table 5). The best results are again achieved by ResNet and ViT with 97% and 96% average F1-score. The models achieve uniform F1 results for each of the classes, namely ResNet in the range from 93 to 100%, and ViT in a slightly wider range from 86% to 99%. Both models achieve strong macro-average scores and show excellent results for all classes with respect to all metrics except for two, classes 3 and 6 suggesting that their performance is evenly distributed across classes.

Table 5. Evaluation of Models Trained and Tested on Images Sampled from a Fixed Lower-Left Position (UNIRI-SeaState-LL Dataset)

Fine-tuned models	Metrics	Classes								Accuracy	Macr o avg	Weighted avg
		1	2	3	4	5	6	7	8			
ResNet	precision	1.000	0.941	0.911	0.981	0.996	0.952	1.000	0.944	0.974	0.966	0.975
	recall	0.964	1.000	0.959	0.962	0.986	0.936	1.000	1.000	0.974	0.976	0.974
	f1-score	0.981	0.970	0.934	0.971	0.991	0.944	1.000	0.971	0.974	0.970	0.974
ViT	precision	0.997	0.966	0.777	0.991	0.989	0.899	0.983	0.943	0.955	0.943	0.959
	recall	0.990	0.997	0.955	0.899	0.964	0.911	1.000	0.988	0.955	0.963	0.955
	f1-score	0.993	0.981	0.857	0.942	0.976	0.905	0.991	0.965	0.955	0.951	0.956
MobileNet	precision	0.991	0.789	0.615	0.921	0.979	0.508	0.972	0.851	0.844	0.828	0.870
	recall	0.875	0.934	0.861	0.722	0.898	0.647	1.000	0.952	0.844	0.861	0.844
	f1-score	0.929	0.855	0.718	0.810	0.937	0.569	0.986	0.899	0.844	0.838	0.850
NASNet	precision	1.000	0.879	0.814	0.934	0.976	0.626	0.988	0.932	0.902	0.894	0.915
	recall	0.917	0.983	0.788	0.856	0.916	0.877	0.994	0.976	0.902	0.913	0.902
	f1-score	0.957	0.928	0.801	0.893	0.945	0.730	0.991	0.953	0.902	0.900	0.905

The other models for the same classes also show the worst performance. But, although NASNet has 10 and 20 times fewer parameters than the ResNet and ViT networks, respectively, for 6 out of 8 classes they achieve an F1 score above 90%, while for classes 3 and 6, for which the mentioned models have somewhat lower accuracy, they achieve an F1 score of 80% and 73%, which is a respectable result considering the complexity of the task.

MobileNet is significantly the smallest network, with the smallest number of parameters and with twice as many iterations as the best networks it manages to achieve satisfactory results with an 85% average F1 score which shows that it can be used successfully on edge devices with limited computing resources.

Analysis of performance metrics in Table 5 reveals that all models, despite different architectures and number of parameters, show potential for high performance in sea state classification, taking into account not only overall accuracy, but the impact of class distribution on these measures and performance for each individual class.

ResNet evaluation on MU-SSiD dataset

The MU-SSiD dataset [Umair et al. \(2022\)](#) is a publicly available dataset of sea state images in four classes from 1-4 Bft. The dataset contains 6000 images per class cropped from a source video in full HD resolution, similarly as in our dataset.

We trained the ResNet model that performed best on our dataset on the MU-SSiD dataset using the same training setup as when training on the UNIRI-SeaState-LL dataset, only with the adjusted number of classes in the final layer, 4 in this case. In the following, we refer to this model as ResNet-Mu-SSiD. We compared the performance of the models trained on one dataset on the other dataset. Namely, we test the ResNet model trained on the UNIRI-SeaState-LL dataset (ResNet-UNIRI) on the UNIRI-SeaState-LL and MU-SSiD datasets, and we test the ResNet-Mu-SSiD on both the UNIRI-SeaState-LL and MU-SSiD datasets. The goal of this experiment was to determine if the models are applicable on dataset taken in very different settings.

The results for the ResNet-Mu-SSiD model are shown in Table 6. The model performs well when tested on the dataset similar to one it was trained on, and similarly to the reported results in [Umair et al. \(2022\)](#). However, on the UNIRI-SeaState-LL dataset it shows a significant drop in performance, from 78% accuracy to 31% accuracy.

Table 6. Evaluation of ResNet Model trained on MU-SSiD training dataset and tested on both test set of the MU-SSiD and test set of the UNIRI-SeaState-LL

Test set	Metrics	Classes				Accuracy	Weighted avg	Performance drop
		1	2	3	4			
MU-SSiD	precision	0,93	0,59	0,67	0,99		0,7928	-
	recall	0,77	0,68	0,67	1	0,78	0,7794	-
	f1-score	0,84	0,63	0,67	0,99		0,7833	-
UNIRI-SeaState-LL	precision	0,21	0,43	0,67	0,63		0,491	0,3
	recall	0,48	0,85	0,12	0,02	0,31	0,3133	0,47
	f1-score	0,29	0,57	0,21	0,04		0,2339	0,55

The results for the ResNet-UNIRI model are shown in Table 7. Similarly as the ResNet-Mu-SSiD model, the model performs well when tested on the dataset test subset of dataset it was trained on. Again, the performance drops significantly when tested on different dataset (MU-SSiD), down

to 28% accuracy from 88% accuracy. It can be noted that this model was trained on 8 classes, and thus could classify an image from the test set into classes that were not present in the dataset at all (5-8 Bft).

Table 7. Evaluation of ResNet Model trained on UNIRI-SeaState-LL training dataset and tested on both test set of the MU-SSiD and test set of the UNIRI-SeaState-LL

Test set	Metrics	Classes								Accuracy	Weighted average	Perform. drop
		1	2	3	4	5	6	7	8			
UNIRI-SeaState-LL	precision	1	0,9	0,54	0,92	1,00	0,80	0,96	0,88	0,91		
	recall	0,93	0,98	0,93	0,86	0,80	0,82	1,00	0,91	0,88		
	f1-score	0,96	0,94	0,68	0,89	0,89	0,81	0,98	0,89	0,89		
MU-SSiD	precision	1	0,4	0,78	0	0	0	0	0	0,55	0,36	
	recall	0,05	0,91	0,14	0	0	0	0	0	0,28	0,61	
	f1-score	0,09	0,56	0,24	0	0	0	0	0,28	0,22	0,67	

The confusion matrix for ResNet-UNIRI tested on the MU-SSiD dataset (Table 8), shows the problem of misclassification. For example, many instances of class 4 in the MU-SSiD dataset were classified as class 7. Also, many instances of class 3 were classified as class 2. The reason for both of these errors might be explained with the difference of data collection, primarily the camera position and height. Since the images in the UNIRI-SeaState-LL dataset were taken from much greater height, the difference between calmer sea states e.g. 2 and 3 are not as pronounced as when captured from 2-3 m.

Table 8. Confusion matrix of ResNet Model trained on UNIRI-SeaState-LL training dataset and tested on the MU-SSiD test set

True class	Predicted class							
	1	2	3	4	5	6	7	8
1	56	655	47	1	35	238	4	164
2	0	1091	2	0	19	15	0	73
3	0	945	173	12	0	69	0	1
4	0	13	0	0	0	0	1187	0
5	0	0	0	0	0	0	0	0
6	0	0	0	0	0	0	0	0
7	0	0	0	0	0	0	0	0
8	0	0	0	0	0	0	0	0

The authors of (MU-SSiD) state that the raw videos for their dataset were captured at a height of 2 to at most 12m, while our dataset was formed from videos taken at height of about 40m, or more than 4 times higher. Thus, the waves of e.g. sea state 4 appear visually much smaller on our dataset, and waves of sea state 7 in our dataset visually appear similar to sea state 4 taken from much lower height as in MU-SSiD dataset (Fig. 11).

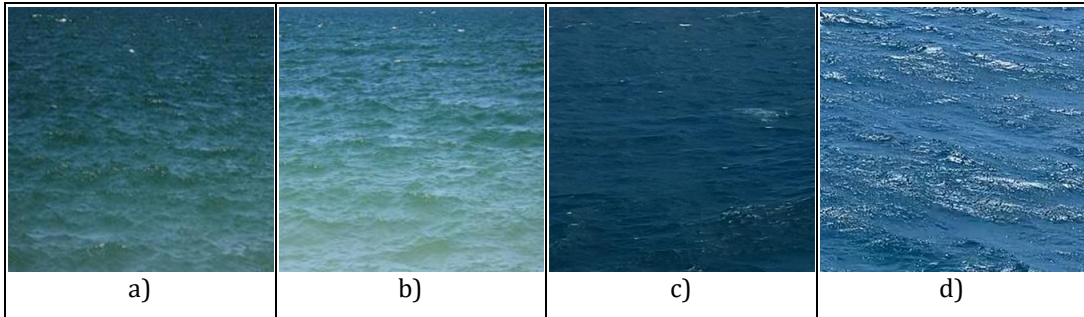


Figure 11. a), b) samples of sea state 4 in MU-SSiD dataset; c), d) samples of sea state 7 in UNIRI-SeaState-lower-left-331 dataset.

The obtained results confirm that the models are very dependent on the recording conditions, especially height, so if the models should be used on ships of different sizes, this problem should be addressed in the future.

Discussion

The comparative analyses of model performance based on images sampled from fixed and random positions has revealed several key considerations for the classification of sea states.

The empirical results show that the models trained on the set of images from a fixed lower-left position, achieve better results than those trained on randomly sampled images. This may be ascribed to the greater consistency of wave appearance within classes, because due to the camera angle and the distance to the camera, the wave sizes vary highly within the video frame and farther images of a class may be visually similar to near image of another class. This points to the limitation of the models that are dependent on the camera height, distance, and orientation. This is further confirmed with training and testing on datasets that were taken from different heights, where the models trained on data from one height were not able to successfully recognize the sea state taken from very different height. Further studies should explore whether a general model for sea state classification that is tolerant of camera position change is feasible or different models should be trained for different heights.

It emerges that while the inherent complexity of a model, inferred from the quantity of its parameters, contributes to the granularity of data interpretation, the image sampling strategy exerts a comparable influence on the performance metrics. A deliberate approach to the collection of training data, which encompasses not only a comprehensive spectrum of sea states but also other factors such as camera position, time of day etc. is important for improving the robustness and universality of these models.

An opportunity also exists to improve the model accuracy, especially within the ambit of sparsely represented sea states by targeted augmentation of the dataset with additional instances from these less prevalent conditions.

Looking ahead, we aim to extend the dataset to capture a wider variety of sea states and to continuously refine our model. This progression will allow us to further solidify the models' performance, ensuring accurate sea state recognition that is vital for safe and efficient maritime operations.

4. Conclusion

This research explores the application of computer vision and deep learning to the automated real-time classification of sea states, contributing to the field of maritime safety and vessel energy efficiency. Advanced models, including transfer learning have effectively categorized sea states within the operational envelope based on the Beaufort scale.

As part of the research, relevant video data of the state of the sea were collected and two sets UNIRI-SeaState-LL and UNIRI-SeaState-R of data were formed, sampled from the video according to different strategies and prepared for supervised machine learning of the model. The sets cover eight classes of sea state within an operational framework based on the Beaufort scale, each marked from 1 to 8.

We selected state-of-the-art models of deep neural networks of different architectures and parameter ranges from 2.7 to 87 M, MobileNet, NASNet, ResNet and ViT and fine-tuned them using transfer learning and a custom data set to recognize different sea states.

To determine the most effective models for sea state classification we tested and compared the performance of the model according to the standard metrics of precision, recall, F1 score, and accuracy, taking into account macro and weighted average results.

Our research showed that the best results according to all metrics, taking into account the macro and weighted average results, were achieved by the ResNet model with an average F1 score of 97%. The ViT model, which has twice as many parameters, achieved comparative results with an average F1 score of 95.6%. Two other networks with a significantly smaller number of parameters, in the range of 10-40 times less, also achieved good results, the average F1-score for NASNet was 90% and for MobileNet 85%.

The study also analysis the model performances based on image samples from fixed versus random positions and showed that the image sampling strategy affects the classification results. Models trained with images from a stable, fixed vantage point consistently outperformed those trained on randomly sampled images, which emphasizes the importance of a stable image perspective in enhancing model learning capabilities.

Also, testing the model on image sets that were collected with different shooting setups, especially significantly different shooting heights, confirm that shooting height has a significant impact on model performance. The reason for this is that the visual features of the same sea state look different at different recording heights, moreover, recordings from buoys or smaller ships of just rough seas visually correspond to recordings of stormy and very wavy seas when taken from ocean liners.

The implications of this research are particularly relevant to the growing field of autonomous navigation, where real-time assessment of navigational conditions is critical to the safety and efficiency of unmanned maritime vessels. As the industry moves towards more autonomous operations, the ability to accurately predict and adapt to changing sea conditions becomes increasingly important.

In future work, we aim to extend our research to include regression analysis, which will allow us to predict sea state conditions as a continuous variable, providing deeper insights into the maritime environment. In addition, we will try to investigate whether it is possible to create a model for classifying the sea state that takes into account the shooting height or is invariant to it. This would enable the creation of a general model that has good performance at different recording positions and heights, so different models should not be fine-tuned for different ships.

Acknowledgments

This research was partially supported by HORIZON EUROPE Widening INNO2MARE project (grant agreement ID: 101087348).

References

Ampilova, N., Soloviev, I., Kotopoulos, A., Pouraimis, G., & Frangos, P. (2019). On the application of multifractal methods for the analysis of sea surface images related to sea state

determination. *CEMA Engineering Conference 2019*. Sofia: CEMA. Retrieved 05 20, 2023, from http://rcvt.tusofia.bg/CEMA2019_8.pdf

Bouman, E. A., Lindstad, E., Rialland, A. I., & Strømman, A. H. (2017). State-of-the-art technologies, measures, and potential for reducing GHG emissions from. *Transportation Research Part D: Transport and Environment*, 408-421. doi:10.1016/j.trd.2017.03.022

Cheng, X., Li, G., Skulstad, R., Chen, S., Hildre, H. P., & Zhang, H. (2019). Modeling and Analysis of Motion Data from Dynamically Positioned Vessels for Sea State Estimation. *IEEE International Conference on Robotics and Automation* (pp. 6644-6650). IEEE. doi:10.1109/ICRA.2019.8794069

Deng, J., Dong, W., Socher, R., Li, L.-J., Li, K., & Fei-Fei, L. (2009). Imagenet: A large-scale hierarchical image database. *2009 IEEE conference on computer vision and pattern recognition*, (pp. 248-255).

He, K., Zhang, X., Ren, S., & Sun, J. (2016). Deep residual learning for image recognition. *Proceedings of the IEEE conference on computer vision and pattern recognition*, (pp. 770-778).

Kolesnikov, A., Dosovitskiy, A., Weissenborn, D., Heigold, G., Uszkoreit, J., Beyer, L., . . . Zhai, X. (2021). An Image is Worth 16x16 Words: Transformers for Image Recognition at Scale.

Li, J., Xu, C., Su, H., Gao, L., & Wang, T. (2022). Deep Learning for SAR Ship Detection: Past, Present and Future. (D. Gleich, Ed.) *Remote Sensing*, 14, 2712. doi:10.3390/rs14112712

Lin, T.-Y., Maire, M., Belongie, S., Hays, J., Perona, P., Ramanan, D., . . . Zitnick, C. L. (2014). Microsoft coco: Common objects in context. *Computer Vision-ECCV 2014: 13th European Conference, Zurich, Switzerland, September 6-12, 2014, Proceedings, Part V 13*, (pp. 740-755).

Lindstad, H., Verbeek, R., Blok, M., Zyl, S. v., Hübscher, A., Kramer, H., . . . Boonman, H. (2015). *GHG emission reduction potential of EU-related maritime transport and on its impacts*. Delft: TNO. Retrieved 06 29, 2023, from https://climate.ec.europa.eu/system/files/2016-11/report_ghg_reduction_potential_en.pdf

Mittendorf, M., Nielsen, U. D., Bingham, H. B., & Storhaug, G. (2022). Sea state identification using machine learning—A comparative. *Ocean Engineering*, 244. doi:10.1016/j.marstruc.2022.103274

Moosbauer, S., Koenig, D., Jaekel, J., & Teutsch, M. (2019). A Benchmark for Deep Learning Based Object Detection in Maritime Environments. *IEEE/CVF Conference on Computer Vision and Pattern Recognition (CVPR) Workshops* (pp. 0-0). Computer Vision Foundation. Retrieved 04 20, 2023, from https://openaccess.thecvf.com/content_CVPRW_2019/html/PBVS/Moosbauer_A_Ben_chmar

Nielsen, U. D., Bjerregård, M., Galeazzi, R., & Fosser, T. I. (2015). New Concepts for Shipboard Sea State Estimation. *OCEANS '15* (pp. 213-223). DTU. doi:10.23919/OCEANS.2015.7404386

Qiao, D., Liu, G., Lv, T., Li, W., & Zhang, J. (2021). Marine Vision-Based Situational Awareness Using Discriminative Deep Learning: A Survey. (F. Ronan, Ed.) *Journal of Marine Science and Engineering*, 9,397. doi:doi.org/10.3390/jmse9040397

Rus, M., Fettich, A., Kristan, M., & Ličer, M. (n.d.). HIDRA2: deep-learning ensemble sea level and storm tide forecasting in the presence of seiches – the case of the northern Adriatic. *Geosci. Model Development*, 16, 271–288. doi:10.5194/gmd-16-271-2023

Ruth, E., & Thompson, I. (2022). Comparing design assumptions with hindcast wave conditions. *Ocean Engineering*, 247. doi:10.1016/j.oceaneng.2022.110613

Sandler, M., Howard, A., Zhu, M., Zhmoginov, A., & Chen, L.-C. (2018). Mobilenetv2: Inverted residuals and linear bottlenecks. *Proceedings of the IEEE conference on computer vision and pattern recognition*, (pp. 4510–4520).

Tu, F., Ge, S., Choo, Y., & Hang, C. (2018). Sea State Identification Based on Vessel Motion Response Learning via Multi-Layer Classifiers. *Ocean Engineering*, 147, 318–332.

Umair, M., Hashmani, M. A., Rizvi, S. S., Taib, H., Abdullah, M. N., & Memon, M. M. (2022). A Novel Deep Learning Model for Sea State Classification Using Visual-Range Sea Images. *Symmetry*, 14. doi:doi.org/

Vorkapić, A., Radonja, R., & Martinčić-Ipšić, S. (2021). A framework for the application of shipboard energy efficiency monitoring, operational data prediction and reporting. *Pomorstvo*, 35 (1), 3-15. doi:10.31217/p.35.1.1

Vorkapić, A., Radonja, R., & Martinčić-Ipšić, S. (2021, 04). Predicting Seagoing Ship Energy Efficiency from the Operational Data. *Sensors*, 21(8):2832. doi:10.3390/s21082832

Waleed M. Talaat, A. A.-G. (2023). An EEDI based method to better the selection of form and propulsion parameters and improve energy efficiency during preliminary designs of single screw seagoing general/bulk cargo ship. *Ocean Engineering*, 288(1). doi:10.1016/j.oceaneng.2023.116012

Wu, G., Atilla, I., Tahsin, T., Terziev, M., & Wang, L. (2021). Long-voyage route planning method based on multi-scale visibility graph for autonomous. *Ocean Engineering*, 219. doi:/10.1016/j.oceaneng.2020.108242

Zhang, K., Yu, Z., & Qu, L. (2021). Application of Deep Learning in Sea States Images Classification. *7th Annual International Conference on Network and Information Systems for Computers (ICNISC)*, (pp. 976-979). Guiyang. doi:10.1109/ICNISC54316.2021.00183

Zoph, B., Vasudevan, V., Shlens, J., & Le, Q. V. (2018). Learning transferable architectures for scalable image recognition. *Proceedings of the IEEE conference on computer vision and pattern recognition*, (pp. 8697–8710).